Inorganic Chemistry

Article

Cite This: *Inorg. Chem.* 2019, 58, 3316−3328

pubs.acs.org/IC

Control of Excited-State Supramolecular Assembly Leading to Halide Photorelease

Michael D. Turlington, Ludovic Troian-Gautier, Renato N. Sampaio, Evan E. Beauvilliers, and Gerald J. Meyer*

Department of Chemistry, University of North Carolina at Chapel Hill, Murray Hall 2202B, Chapel Hill, North Carolina 27599-3290, United States

Supporting Information

ABSTRACT: Ground- and excited-state control of halide supramolecular assembly was achieved through the preparation of a series of ester- and amide-functionalized ruthenium polypyridyl complexes in CH_2Cl_2. Hydrogen-bonding amide and alcohol groups on the receptor ligand were found to direct interactions with halide, while halide association with the ethyl ester groups was not observed. The various functional groups on the receptor ligands tuned the ground-state equilibrium constants over 2 orders of magnitude (1×10^5 to 1×10^7 M^{-1}), and the fractional contribution of each hydrogen-bond donor to the total equilibrium constant was determined. Pulsed-laser excitation of the complexes resulted in excited-state localization on the ester- or amide-functionalized ligands. In the case where the excited state was oriented toward an associated halide ion (the amide complexes), an 80 ± 10 meV Coulombic repulsion was induced that lowered the excited-state equilibrium constant (K^*_{eq}) and resulted in halide photorelease. The rate constants for excited-state halide release (k^*_{21}) were determined, and the values varied based on the functional groups present in the receptor ligand. Complexes with more hydrogen-bonding donors had smaller rate constants for halide photorelease. In a complex without a specific receptor ligand, the excited-state dipole was not oriented toward the associated halide, and the excited state was therefore found to have a larger equilibrium constant for halide association than the ground state.

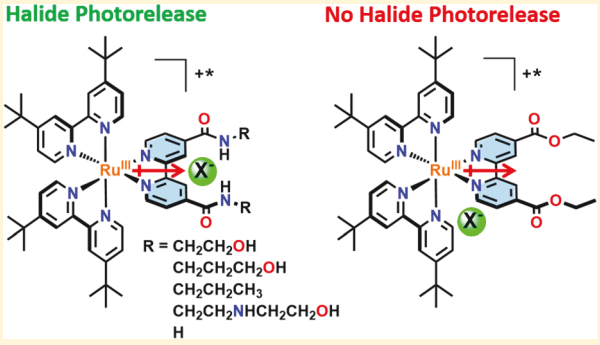

INTRODUCTION

Supramolecular assembly of halides is well-established as a tool for halide sensing,[1] but recent advances have allowed this chemistry to be exploited in a growing array of applications spanning templated synthesis,[2−4] catalysis,[5−8] and halide transport across membranes.[9−14] These applications rely on intermolecular forces like hydrogen and halogen bonding, among others, to facilitate ground-state assembly structures with halides that then perform desired chemistry. Recent work has shown that the formation of ground-state assembly structures between ruthenium polypyridyl complexes and iodide affects the excited-state electron transfer reactivity between the two species.[15,16] These results imply that control over excited-state supramolecular assembly is necessary for influencing the mechanisms and kinetics of important energy-storing reactions. However, to our knowledge, little work has characterized the response of ground-state halide assembly structures to photoexcitation.

Recently, it was reported that equilibrium constants for chloride assembly differed in the ground (K_{eq}) and excited (K^*_{eq}) states.[17] In that report, two ruthenium polypyridyl complexes were designed with a common halide receptor ligand and with a luminescent metal-to-ligand charge-transfer (MLCT) excited state that was oriented toward or away from the associated halide. In heteroleptic Ru(II) complexes, the photoluminescent excited state in fluid solution is known to be localized on the most easily reduced ligand.[17] Hence, when electron-withdrawing CF_3 groups were present on the ancillary ligands, the excited-state dipole was oriented away from the receptor ligand. In contrast, when the ancillary ligands contained electron-donating *t*-butyl groups, the excited-state dipole was oriented toward the receptor ligand. The excited-state localization had little effect on the assembly structure or the ground-state equilibrium constants (K_{eq}) with chloride. When the excited state was localized on the halide receptor ligand, photoexcitation reduced the equilibrium constant (K^*_{eq}) by a factor of 20, which resulted in chloride photorelease. Conversely, when the excited state was localized away from the associated halide, the K^*_{eq} value was increased by 45-fold. These results showed that molecular excited states provide novel control over halide supramolecular assembly that could enable future applications with visible light in seawater desalination and cystic fibrosis-related diseases.[18−20]

Herein, the ground- and excited-state properties that contribute to halide photorelease are more thoroughly

Received: December 4, 2018
Published: February 15, 2019

DOI: 10.1021/acs.inorgchem.8b03383
Inorg. Chem. 2019, 58, 3316−3328

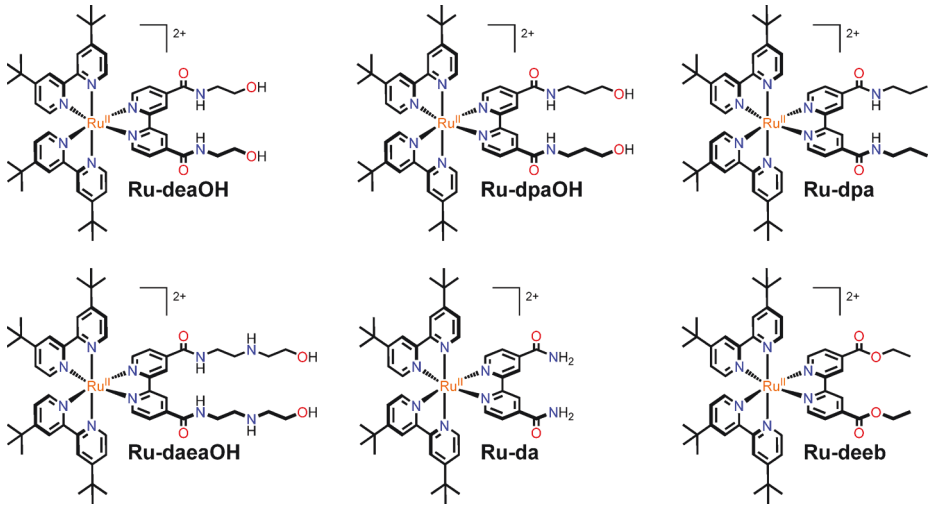

Figure 1. Ruthenium polypyridyl complexes for supramolecular assembly with halides used in this study. The ligand abbreviations (deaOH, dpaOH, dpa, daeaOH, da, deeb) are descriptive of the substituents in the 4,4′ position of the amide- or ester-functionalized ligands. The lowercase letters describe the length of the alkyl chain (e.g., dea = diethylaminde, dpa = dipropylamide), while an uppercase OH when present indicates a terminal alcohol.

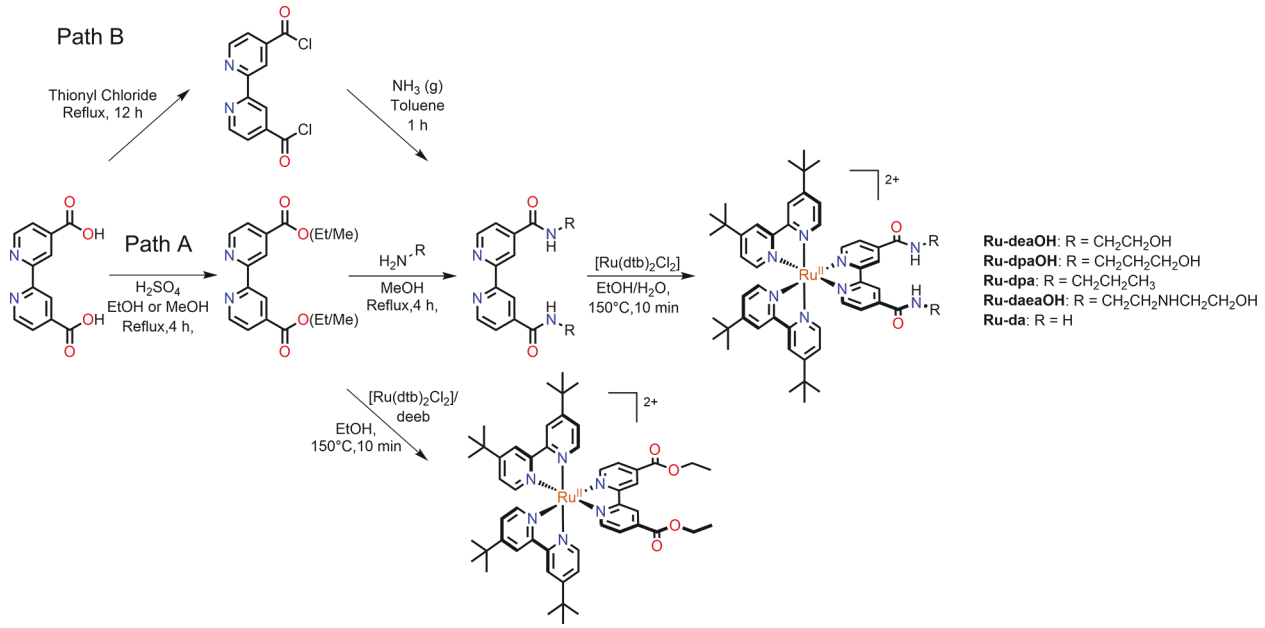

Figure 2. Synthetic pathway used to prepare the discussed complexes. See Experimental Section for additional details.

investigated. Toward this end, a series of six ruthenium complexes (Figure 1) for supramolecular assembly with chloride and bromide are presented. As reported previously, iodide quenched the ruthenium excited state, which precluded a detailed characterization of photorelease with this halide.[15] In this series of complexes, the functional groups on the halide receptor ligands were systematically varied, while the ancillary ligands remained constant. All complexes formed strong ground-state assembly structures with chloride and bromide in CH_2Cl_2. Functional-group variations on the receptor ligands tuned the equilibrium constants across 2 orders of magnitude, and the fractional contribution of each functional group to the total equilibrium constant was determined. Excitation of the amide-functionalized halide assemblies resulted in a Coulombic repulsion between the halide and the excited state that facilitated halide release. The rate constants for this dissociation were sensitive to the hydrogen-bond donors on the receptor ligand, indicating that hydrogen-bonding interactions provide a significant barrier to halide photorelease. These results, which reveal molecular design principles that can be used to control excited-state supramolecular assembly, are discussed in relationship to applications that involve halide release in polar solvents.

RESULTS

The synthetic pathway for the complexes discussed herein is shown in Figure 2. The amide-containing bipyridine ligands (**deaOH**, **dpaOH**, **dpa**, and **daeaOH**) were obtained by refluxing 4,4′-diethylester-2,2′-bipyridine (**deeb**) or 4,4′-dimethylester-2,2′-bipyridine (**dmeb**) and a large excess of the appropriate amine in methanol for 4 h. The yields ranged from 54 to 92% (Figure 2, Path A). Ligand **da** was synthesized

DOI: 10.1021/acs.inorgchem.8b03383
Inorg. Chem. 2019, 58, 3316−3328

Table 1. Photophysical Properties of the Complexes and their Ion-Paired Analogues in CH_2Cl_2

complex	K_{eq} (M^{-1})	K^*_{eq} (M^{-1})	λ_{max} PL (nm)	τ (μs)	Φ_{PL}	k_r ($\times 10^4$ s^{-1})	k_{nr} ($\times 10^5$ s^{-1})	E^0 (V vs NHE) $Ru^{III/II}$	E^0 (V vs NHE) $Ru^{2+/+}$
Ru-deaOH			670	1.32	0.083	6.3	7.0	1.68	−0.82
Cl^-	3.6×10^7 [a]	2.4×10^6	645	1.66	0.170	9.0	4.6	1.72	−0.86
Br^-	4.4×10^7 [a]	2.9×10^6	647	1.65	0.120	6.8	4.9		
Ru-dpaOH			668	1.14	0.130	12	7.6	1.56	−0.85
Cl^-	$>1 \times 10^6$ [b]	*c*	643	1.59	0.310	16	3.6	1.60	−0.90
Br^-	$>1 \times 10^6$ [b]	*c*	643	1.66	0.230	14	4.7		
Ru-dpa			667	1.17	0.150	13	7.3	1.60	−0.91
Cl^-	2.8×10^7 [a]	5.7×10^5	633	1.92	0.390	20	3.2	1.67	−0.94
Br^-	8.0×10^6 [a]	2.4×10^5	637	1.88	0.390	21	3.3		
Ru-daeaOH			665	1.18	0.061	5.2	8.0	1.56	−0.88
Cl^-	3.5×10^6	1.6×10^5	643	1.33	0.120	6.8	4.8	1.57	*d*
Br^-	1.7×10^6	2.4×10^5	650	1.60	0.100	6.4	5.6		
Ru-da			677	0.95	0.090	9.5	9.6	1.56	−0.82
Cl^-	5.7×10^5	2.9×10^4	650	1.49	0.250	15	4.4	1.61	−0.97
Br^-	5.6×10^5	2.9×10^4	650	1.57	0.220	14	5.0		
Ru-deeb			688	1.03	0.081	7.9	8.9	1.62	−0.68
Cl^-	9.7×10^4	2.1×10^5	696	0.87	0.067	7.7	11	1.66	−0.67
Br^-	1.0×10^5	2.2×10^5	695	0.87	0.067	7.7	11		

[a]Determined through competitive binding experiments. [b]Equilibrium constant was too large to be measured, and no suitable competitor was found; therefore, a minimum is given. [c]As K_{eq} could not be determined, K^*_{eq} could not be calculated. [d]Could not be determined.

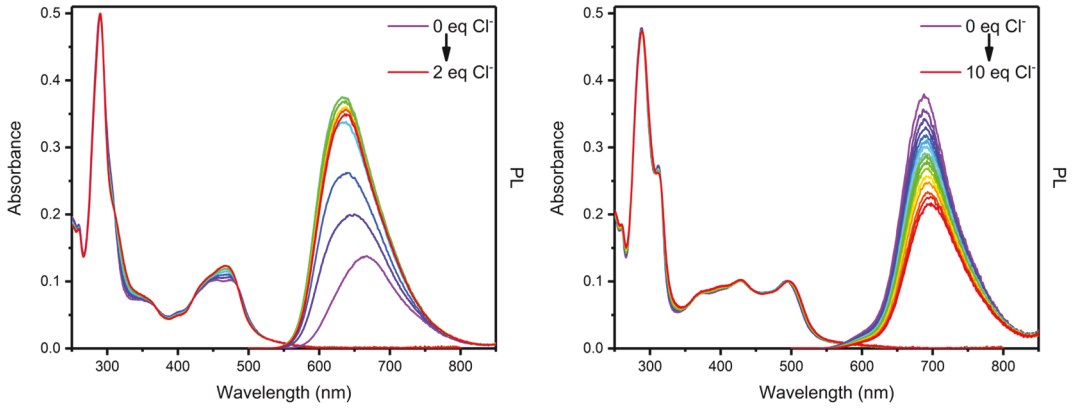

Figure 3. Absorbance and photoluminescence (PL) (λ_{ex} = 450 nm) spectra of **Ru-dpa** (left) and **Ru-deeb** (right) in CH_2Cl_2 at room temperature as TBA chloride was titrated into solution.

through another route (Figure 2, Path B), wherein 4,4′-dicarboxylic acid-2,2′-bipyridine was refluxed in the presence of thionyl chloride to give the highly reactive acid chloride. The addition of ammonia gas to the dissolved intermediate caused **da** to precipitate. The ruthenium complexes were synthesized by microwave irradiation of $Ru(dtb)_2Cl_2$ (**dtb** = 4,4′-di-*tert*-butyl-2,2′-bipyridine) and the appropriate ligand in EtOH or H_2O/EtOH mixtures and were further isolated as the PF_6^- salt, with yields ranging from 70 to 90% (Figures S1–S19).

Cyclic and square-wave voltammetry in CH_2Cl_2 revealed quasi-reversible $Ru^{III/II}$ and ligand-based reductions for all complexes. For the amide-derivatized complexes, the first ligand-based reduction fell within a narrow range from −820 to −910 mV versus normal hydrogen electrode (NHE), while the first reduction of **Ru-deeb** occurred at −680 mV. The metal-centered $Ru^{III/II}$ potentials of all complexes spanned from 1560 to 1680 mV (Table 1).

The UV–visible absorption spectra of all complexes in CH_2Cl_2 were typical of ruthenium polypyridyl complexes. The broad absorption bands from 400 to 500 nm were ascribed to MLCT transitions, while the features at or below 300 nm were assigned to ligand-centered transitions. The addition of tetrabutylammonium (TBA) chloride or bromide salts to ∼10 μM solutions of the ruthenium complexes induced changes in the absorption spectra, particularly to the MLCT band (Figures 3 and S20). These changes were manifest primarily as increases in the MLCT intensity of the amide complexes (Figure 3, left), while **Ru-deeb** mainly experienced a red shift of the MLCT band (Figure 3, right). The spectral shifts saturated at high halide concentrations, and a Benesi–Hildebrand type analysis of the absorbance changes gave ground-state equilibrium constants (K_{eq}) ranging from 1×10^5 to more than 1×10^6 M^{-1} (Table 1).[21,22] For complexes **Ru-deaOH**, **Ru-dpaOH**, and **Ru-dpa**, the binding isotherms were so steep ($>1 \times 10^6$ M^{-1}) that K_{eq} values could not be resolved through standard UV–vis titrations, and so competitive binding experiments were performed.[23,24] The ions TBA triflate (Figure S21) and TBA tetrafluoroborate (Figure S22) were found to be suitable competitors for **Ru-deaOH** and **Ru-**

DOI: 10.1021/acs.inorgchem.8b03383
Inorg. Chem. 2019, 58, 3316–3328

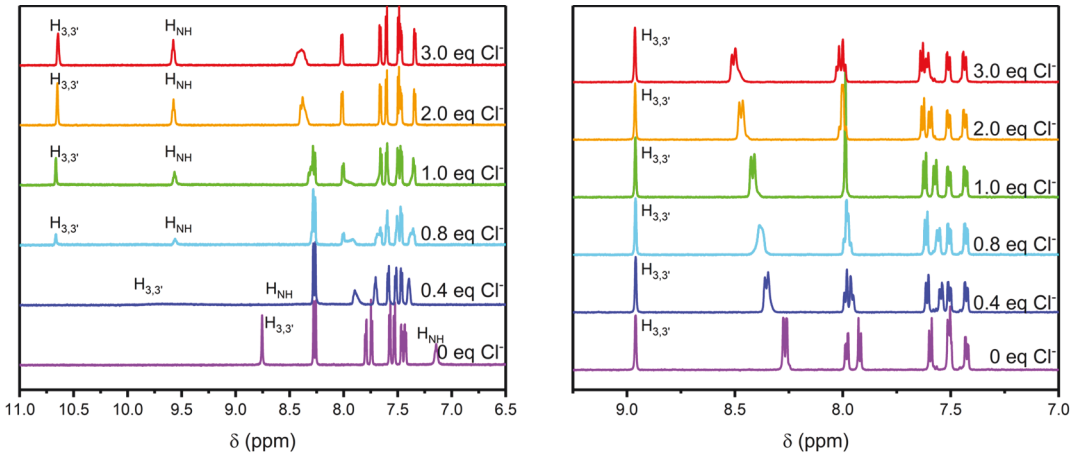

Figure 4. Aromatic region of the ^{1}H NMR spectra of **Ru-dpa** (left) and **Ru-deeb** (right) as chloride was titrated into CD_2Cl_2. The $H_{3,3'}$ label designates the 3,3′ hydrogens on the dpa (left) or deeb (right) ligands.

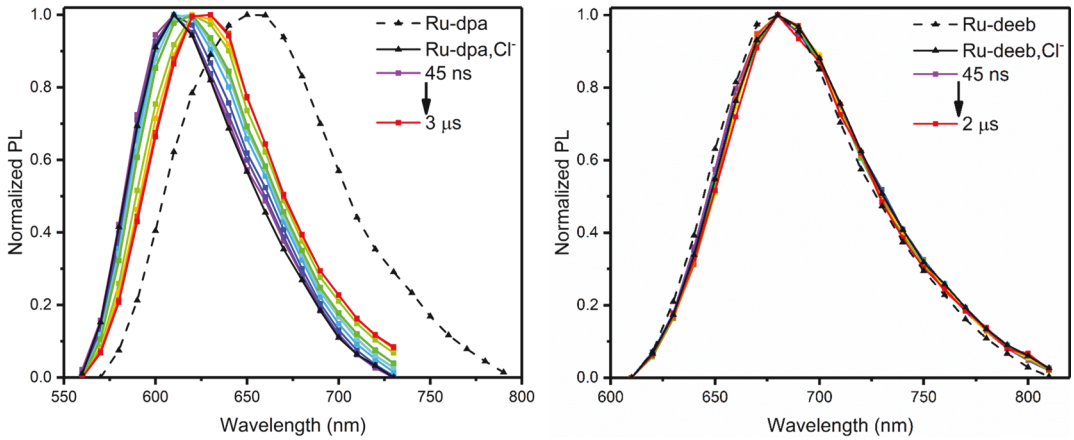

Figure 5. PL spectra of **Ru-dpa** (left) and **Ru-deeb** (right) measured at 45 ns and longer time delays after pulsed 500 nm excitation in the presence of 1 equiv of chloride in CH_2Cl_2. For reference, the PL spectra of the non-ion-paired complexes are included (black ▲, dashed line).

dpa, respectively, and displayed one-to-one binding with the ruthenium complexes with an equilibrium constant (K_{comp}) in the 1×10^4 to 1×10^5 M^{-1} range. In competitive binding experiments, a fixed concentration of the competitor was present as the halide was titrated into the solution. This competitive equilibrium allowed the desired equilibrium constant to be quantified with eq 1.[23,24] As expected, increasing the competitor concentration from 200 μM (50 equiv) to 1 mM (200 equiv) progressively reduced the observed equilibrium constant (K_{obs}) with halides (Table S1) and gave within error the same values for the calculated K_{eq}.

$$K_{eq} = K_{obs}(1 + K_{comp}[comp]) \quad (1)$$

Titrations of chloride and bromide into 1 mM ruthenium solutions in CD_2Cl_2 were monitored by ^{1}H NMR spectroscopy (Figures 4 and S23). For the amide-functionalized complexes, the 3,3′ hydrogens on the amide-functionalized ligand, as well as the amide hydrogens, displayed large downfield shifts as halide was added to the solution. At halide concentrations between 0 and 1 equiv, significant broadening of these resonances was observed. Additionally, for **Ru-deaOH** and **Ru-dpaOH**, the hydroxyl resonances also drastically shifted downfield. The remaining aromatic and aliphatic resonances did not experience significant shifts in the presence of halide. With **Ru-deeb**, the analogous chloride and bromide titrations produced vastly different results, where the most significant shifts corresponded to the simultaneous deshielding of the 3,3′ hydrogens on the dtb ligand and the 6,6′ hydrogens on the deeb ligand. Significantly, the 3,3′ hydrogens on the deeb ligand did not shift during the course of the titration. The spectral changes for the amide complexes saturated after the addition of ∼1 equiv of halide, which was indicative of 1:1 contact ion pair formation. The 3,3′ dtb hydrogens of **Ru-deeb** continuously shifted even up to 3 equiv of halide, but a Job plot (Figure S24) revealed that this complex also forms a 1:1 ion pair.[25] These data provided no evidence for halide interactions with the deeb ligand in these CD_2Cl_2 solutions.[22,26]

Steady-state and time-resolved photoluminescence (PL) were used to study the excited states of the free and ion-paired complexes. Upon absorption of visible light, all complexes displayed room-temperature PL with maximum ranging from 665 to 688 nm. The steady-state PL spectra of the complexes were sensitive to the halide concentration (Figures 3 and S20). For the amide-containing complexes, the PL spectrum blue-shifted and experienced a 2- to 3-fold increase in intensity with increasing chloride or bromide concentrations, corresponding to an increase in the PL quantum yield. These changes typically saturated between 1 and 2 equiv of halide. For **Ru-deeb**, the addition of chloride

DOI: 10.1021/acs.inorgchem.8b03383
Inorg. Chem. 2019, 58, 3316−3328

and bromide quenched the PL and caused a slight red shift in the spectra.

The PL maximum of the free and ion-paired complexes was taken as a crude estimate of the free energy stored in the excited state (ΔG_{ES}). These values (Table 1) in conjunction with the ground-state K_{eq}, allowed the excited-state equilibrium constants (K^*_{eq}) to be calculated through Förster cycle analysis (Figure S25). For the amide-functionalized complexes, equilibrium constants for halide ion pairing decreased upon excitation, but for **Ru-deeb**, K^*_{eq} was greater than K_{eq}.

The excited-state decay data were well-described by a first-order kinetic model and yielded lifetimes τ on the order of a microsecond. However, the addition of halide to the amide complexes yielded kinetics that were no longer first-order but which were instead successfully modeled by biexponential kinetics. Excited-state quenching was excluded as the cause of this kinetic behavior, as the complexes were not strong enough photo-oxidants to oxidize chloride or bromide.[27−29] Additionally, a biexponential fit using a weighted average of the lifetime of the free and ion-paired species (Ru^{2+} and $[Ru^{2+}, X^-]^+$) did not model the kinetic data. When a large excess of halide was present (from 100 to 200 equiv), first-order decay kinetics were recovered, from which the lifetime of the ion-paired complexes was obtained. Ion pairing was found to increase the excited-state lifetime by 200−500 ns.

The biexponential decay kinetics at intermediate halide concentrations were further probed through transient PL experiments (Figure S26) and were found to report on the excited-state equilibrium, as predicted by the square-scheme discussed below. With 1 equiv of chloride or bromide present, the PL of the amide complexes was found to red shift with time after pulsed laser excitation (Figures 5 and S27). Note that the PL maxima obtained in the transient experiments were not the same as those described in Table 1 or Figure 3, as the transient spectra were not corrected for the instrument response. The transient kinetic data were successfully modeled using a square-scheme kinetic analysis to determine the forward (k^*_{12}) and reverse (k^*_{21}) rate constants for ion pairing in the excited state.[17,30−34]

For **Ru-deeb**, the time-resolved PL data remained single exponential even in the presence of halide, although a decrease in the lifetime was observed. In previous reports, this behavior was attributed to an average lifetime arising from the mixture of the free and ion-paired species, which had similar excited-state lifetimes.[22] With the methods described in these reports, K^*_{eq} for [**Ru-deeb**,Cl^-]$^+$ was calculated to be 2.1×10^5 M^{-1}.[22,35] This value was in good agreement with that obtained from a Förster cycle. Transient PL experiments did not reveal time-dependent shifts in the PL, so the kinetics of the excited-state equilibrium could not be resolved.

DISCUSSION

The experimental data clearly indicate that the ground- and excited-state equilibrium constants for halide binding can be controlled through molecular design. The results are in agreement with a recent study that reported how visible light excitation can be utilized to photorelease chloride ions, provided that the excited state was localized on a bipyridine ligand with an associated chloride ion.[17] This comparative study was undertaken to understand the generality of the previous report and to better understand how functional group variation at the receptor ligand influences the ground- and excited-state equilibrium.

A useful starting point for considering these equilibria is the square scheme shown in Figure 6. The standard Gibbs free

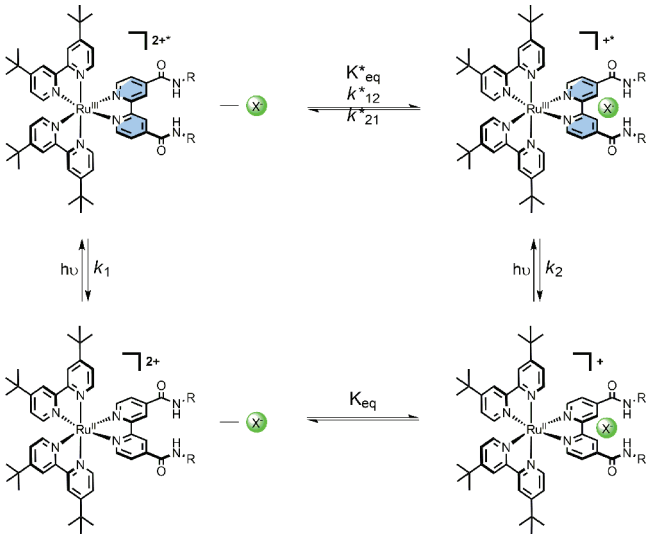

Figure 6. Square scheme for ground- and excited-state equilibria with halides (green sphere), that also depicts the excited-state localization (blue shading). Note that the absorption of light promotes excitation to the Franck−Condon excited state, which then undergoes fast vibrational relaxation and intersystem crossing to the photoluminescent excited state. For simplicity, the square scheme only represents the singlet ground state and the photoluminescent excited state, which are assumed to be the only relevant states in halide binding and photorelease.

energy changes for the ground and excited states of the six complexes investigated are reported in Table 2. Related square schemes have been widely used to quantify the excited-state pK_a values of photoacids and -bases, as well as excimer and

Table 2. Kinetic and Thermodynamic Parameters

complex	ΔG^0_{GS} eV	ΔG^0_{ES} eV	$\Delta G^0_{GS} - \Delta G^0_{ES}$ eV	k^*_{12} M^{-1} $s^{-1}(\times 10^{11})$[a]	k^*_{21} $s^{-1}(\times 10^5)$
Ru-deaOH					
$+Cl^-$	−0.45	−0.38	−0.07	2.4	2.3
$+Br^-$	−0.45	−0.38	−0.07	2.2	1.5
Ru-dpa					
$+Cl^-$	−0.44	−0.34	−0.10	2.2	4.5
$+Br^-$	−0.41	−0.32	−0.09	1.7	6.4
Ru-daeaOH					
$+Cl^-$	−0.39	−0.31	−0.08	1.8	9.1
$+Br^-$	−0.37	−0.32	−0.05	2.1	8.7
Ru-da					
$+Cl^-$	−0.34	−0.26	−0.08	1.3	47
$+Br^-$	−0.34	−0.26	−0.08	0.6	16
Ru-deeb					
$+Cl^-$	−0.30	−0.32	0.02	*b*	*b*
$+Br^-$	−0.30	−0.32	0.02	*b*	*b*

[a]The k^*_{12} values on the order of 1×10^{11} M^{-1} s^{-1} are consistent with a diffusion-limited rate, as calculated in the appendix of the Supporting Information. [b]As the time-resolved PL did not provide evidence for differing ground- and excited-state equilibria, the kinetic analysis could not be performed.

DOI: 10.1021/acs.inorgchem.8b03383
Inorg. Chem. 2019, 58, 3316−3328

exciplex formation.[30−34] Note that in the square scheme in Figure 6, hυ refers to light population of the photoluminescent excited state. Indeed, this is a simplification, as light absorption creates a Franck−Condon state that subsequently relaxes to the photoluminescent state through vibrational relaxation and intersystem crossing. For all the ruthenium complexes reported here, the ground-state equilibrium with chloride and bromide is highly favored in CH_2Cl_2, and the free energies of halide binding provide insights into halide coordination chemistry. In the thermally equilibrated excited state, the square scheme kinetic analysis and the corresponding differential rate equations (eqs 2 and 3, where A is Ru^{2+} and B is Ru^{2+},X^-) are used to model the experimental data. The analytical solutions for these differential rate equations have been derived elsewhere[31−33] and are here used to determine the excited-state equilibrium constant and the forward (k^*_{12}) and reverse (k^*_{21}) rate constants. Significantly, biexponential excited-state decay kinetics, which are predicted by the square scheme,[31−33] are observed here for the amide-functionalized complexes. This discussion of ground- and excited-state supramolecular assembly included in the broader context of halide assembly indicates that control of the ground- and excited-state equilibria with halide can lead to practical applications and fundamental insight into halide coordination chemistry.

$$\frac{d[A^*]}{dt} = -(k^*_{12} + k_1)[A^*] + (k^*_{21})[B^*] \quad (2)$$

$$\frac{d[B^*]}{dt} = -(k^*_{21} + k_2)[B^*] + (k^*_{12})[A^*] \quad (3)$$

GROUND-STATE SUPRAMOLECULAR ASSEMBLY

The ruthenium polypyridyl complexes investigated in this study are designed to associate with halides through supramolecular assembly. Toward this end, hydrogen-bonding functional groups[36] such as amides and alcohols are built into the ligand framework to provide a specific site for halide assembly.[37] The cationic charge of each complex, as well as the use of the low dielectric solvent CH_2Cl_2 (ε = 8.93), also facilitate supramolecular assembly. Finally, the ancillary ligands are designed with sterically bulky *t*-butyl groups to block other halide interactions with the molecule. The characteristic spectral features of these complexes are sensitive to chloride and bromide, providing evidence for supramolecular assembly formation.

A powerful technique for resolving the location of the bound halide that also describes the specific hydrogen-bonding interactions that occur within the ion pair is ^{1}H NMR spectroscopy. In previous studies on related complexes, hydrogen bonding with halides was reported to lengthen the covalent bonds that were involved in the hydrogen-bonding interaction, resulting in downfield shifts of specific ^{1}H NMR signals.[15,17,22,27,38,39] The results herein are consistent with that finding. For the complexes with amide-functionalized ligands, the 3,3′ C−H bonds and amide N−H bonds on the receptor ligand are most responsive to halide, whereas for **Ru-deeb**, the 3,3′ hydrogens on the dtb ligand and the 6,6′ hydrogens on the deeb ligand were most influenced. This indicates that supramolecular assembly with halides is highly sensitive to the functional groups present within the molecule. For the amide-derivatized complexes, the amide groups clearly provide a halide binding site. However, for **Ru-deeb**, the halide does not associate with a specific ligand but instead is located between ligands and in close proximity to the positively charged ruthenium. These interactions are depicted in Figure 7.

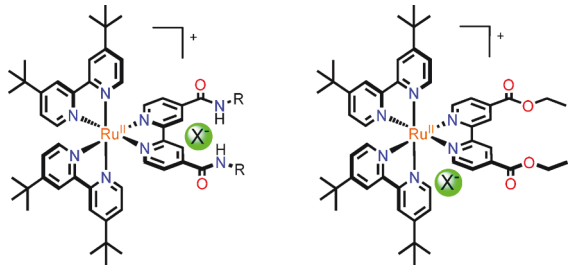

Figure 7. Ion-pairing location for the amide complexes (left) and **Ru-deeb** (right) as determined by ^{1}H NMR spectroscopy.

Table 3. Spectral Shifts of Relevant ^{1}H NMR Signals as Halide is Added

	Δppm					
	$H_{3,3'}$		H_{NH}		H_{OH}	
complex	Cl^-	Br^-	Cl^-	Br^-	Cl^-	Br^-
Ru-deaOH	1.42	1.24	1.68	1.34	1.96	1.12
Ru-dpaOH	1.98	1.35	1.72	1.54	1.17	0.56
Ru-dpa	1.90	1.66	2.44	2.20	N/A	N/A
Ru-daeaOH	1.24	0.99	1.33	1.02	*a*	*a*
Ru-da	1.71	1.54	2.36	2.13	N/A	N/A

[a]Were not observed in the ^{1}H NMR spectrum. N/A indicates not applicable.

The magnitude of the downfield shift (Δppm) of specific resonances in the ^{1}H NMR spectra (Table 3) upon halide addition was found to vary significantly based on the complex and the identity of the halide. It is important to note here that Δppm does not correlate with the equilibrium constant. In other words, the complexes with the largest Δppm do not have the largest K_{eq} values and vice versa. However, in this series of complexes where binding uniformly occurs at the amide-functionalized ligand (excluding **Ru-deeb**), the Δppm value provides insight into functional group effects on the supramolecular assembly. Clearly the 3,3′ C−H, amide N−H, and alcohol O−H (if present) bonds are most significantly affected by the presence of halide. Amide[37,40−45] and hydroxyl[46,47] groups are known to form hydrogen-bonding interactions with anions, and hydrogen bonding with C−H groups, although rare, can also occur when that bond is highly polarized or the binding site is highly structured.[48−51] In **Ru-deeb**, the most likely contributors to hydrogen bonding are the most acidic 3,3′ hydrogens (9.02 ppm) on the deeb ligand. Of the complexes studied herein, the electron-withdrawing ester groups are best able to polarize this 3,3′ C−H bond, and **Ru-deeb** should therefore provide the highest likelihood of hydrogen-bonding interactions at this site. However, halide addition does not perturb these 3,3′ C−H bonds, which suggests that this functional group does not form significant hydrogen-bonding interactions with halides. In the amide derivatives, the 3,3′ C−H bonds are slightly less polarized (9.02−8.81 ppm) than those of **Ru-deeb**, making them even less likely to engage in hydrogen-bonding interactions. The observed halide-induced shifts at this position in the amide complexes are therefore attributed to halide-induced repulsion of electron density in the C−H bond, which deshields the

DOI: 10.1021/acs.inorgchem.8b03383
Inorg. Chem. 2019, 58, 3316−3328

hydrogen atom. The magnitude of this effect is consistent with the distance between the halide and the 3,3′ hydrogens, as discussed below.

As stated previously, hydrogen bonding with amide and alcohol groups is proposed to lengthen the covalent N−H and O−H bonds.[22] For example, **Ru-deaOH** and **Ru-dpaOH** contain the same hydrogen-bonding groups but differ by a single methylene spacer in the aliphatic chain of the amide ligand (Figure 8, right). The O−H bond of **Ru-deaOH** is lengthened more in the presence of halide than that of **Ru-dpaOH**, while the **Ru-dpaOH** N−H bond is elongated more significantly with halide than that of **Ru-deaOH**. This indicates that the length of the aliphatic chain allows the alcohol group on **Ru-deaOH** to interact more fully with halides, which in turn positions the halide farther from the amide group. This analysis is consistent with the electronic repulsion experienced by the 3,3′ C−H bond. In **Ru-deaOH**, the halide is positioned slightly farther from the 3,3′ C−H group, which results in less significant changes to that bond. For **Ru-dpaOH**, the halide is localized closer to the amide group, and the proximity to the 3,3′ C−H bonds increases the electronic repulsion. Complexes **Ru-dpa** (Figure 8, left) and **Ru-da**, which do not contain alcohol groups, provide further evidence for this interpretation. In these complexes, the amide groups are the sole contributors to hydrogen-bonding interactions, and the N−H bond lengths are elongated by nearly 40% more than in the complexes with alcohol groups.

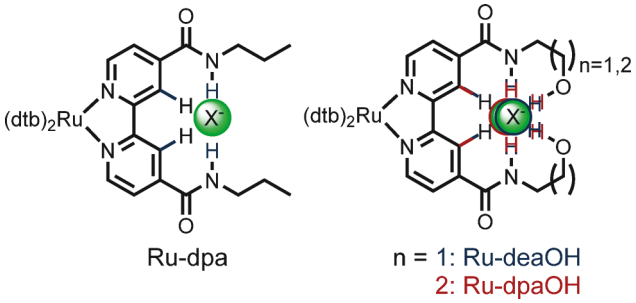

Figure 8. Depiction of the relative C−H, N−H, and O−H bond length changes experienced by **Ru-dpa** (left) and **Ru-deaOH** (blue hydrogens, right) or **Ru-dpaOH** (red hydrogens, right) upon supramolecular assembly with halides. The complexes without alcohol groups (left) have significantly longer amide N−H bonds than the alcohol-containing complexes (right). In complexes with alcohol groups, the changes in O−H and N−H bond lengths trend in opposite directions as the chain length increases from ethyl to propyl.

The ground-state equilibrium constants provide an additional means by which to characterize functional group effects on the supramolecular assembly structure, which is highly favored in all complexes ($K_{eq} \geq 1 \times 10^5$ M^{-1}) in CH_2Cl_2. For **Ru-deaOH**, **Ru-dpaOH**, and **Ru-dpa**, the equilibrium constants for halide binding were so large that they could not be resolved. To overcome this limitation, competitive binding experiments[23,24] (depicted in Scheme 1) were performed to determine the true equilibrium constant. In this work, competitors were sought that displayed a 1:1 stoichiometry with the ruthenium complex and an equilibrium constant that is ∼1 to 2 orders of magnitude less than that of the halide. The presence of a fixed concentration of an appropriate competitor during halide titrations enabled extraction of the desired K_{eq} with halide. Suitable competitors, TBA triflate and TBA tetrafluoroborate, were found for **Ru-deaOH** and **Ru-dpa**, respectively, which allowed for their equilibrium constants with chloride and bromide to be determined using eq 1. An adequate competitor was not found for **Ru-dpaOH**.

The functional groups on the receptor ligands drastically affect the equilibrium constants with halides, which span 2 orders of magnitude and increase in the order of **Ru-deeb** < **Ru-da** < **Ru-daeaOH** < **Ru-dpa** < **Ru-deaOH**. A comparison of the K_{eq} values with chloride (Table 1) enables one to partition the fraction that each functional group contributes to the equilibrium constant. For example, **Ru-deeb**, which

Scheme 1. Equilibrium Constants for Competitive Halide Association with Ru-deaOH and Ru-dpa[a]

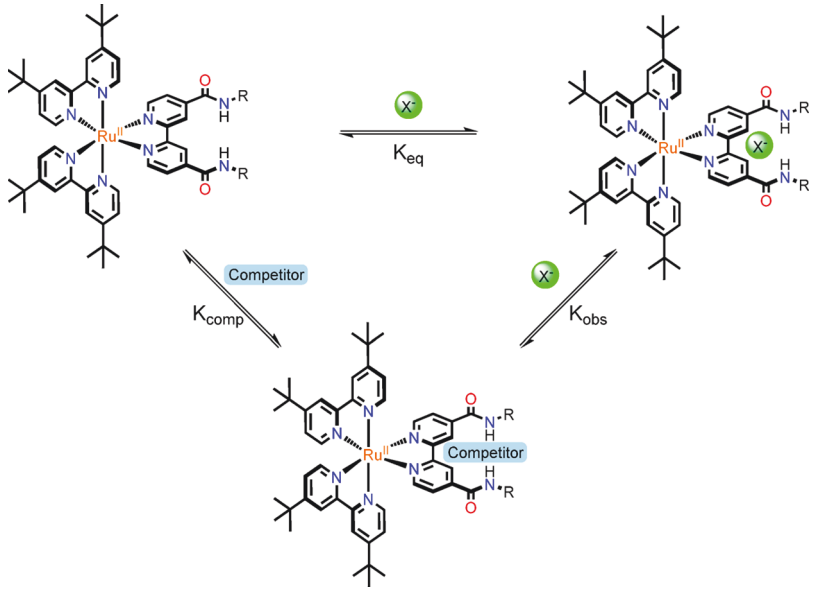

[a]The competitive equilibrium in the presence of a competitor anion and halide experimentally provided an observed equilibrium constant (K_{obs}), which was used to calculate K_{eq} with eq 1.

DOI: 10.1021/acs.inorgchem.8b03383
Inorg. Chem. 2019, 58, 3316−3328

contains two ester groups instead of amide functional groups, displays the weakest equilibrium constant (1×10^5 M^{-1}). As discussed above, this complex does not contain specific functional groups that stabilize halides through a well-defined assembly structure, and so the halide assembly is mainly attributed to the Coulombic attraction with the 2+ charge. Complexes with amide groups, like **Ru-da** and **Ru-dpa**, provide a specific hydrogen-bonding site for halide association, which enhances the K_{eq} by at least a factor of 5. Finally, complexes with alcohol groups on the receptor ligand (**Ru-deaOH** and **Ru-dpaOH**, with the exception of **Ru-daeaOH**) associate so strongly with halides that K_{eq} could not be resolved in the absence of a competitor. These results suggest that the hydrogen-bonding functional groups additively contribute to the K_{eq} values.

The cumulative effect of functional group variation can be seen through a comparison of the ground-state free energies (ΔG°_{GS}) for halide assembly. The complexes **Ru-deeb**, **Ru-dpa**, and **Ru-deaOH** were chosen for this comparison, as the variations in the steric bulk of the receptor ligand are minimal, while the chemical composition of that ligand is changed in a modular fashion. In CH_2Cl_2, the free energy for both chloride and bromide assembly with a 2+ ruthenium polypyridyl complex that does not have a specific receptor ligand for halides (**Ru-deeb**) is −0.30 eV. The addition of hydrogen-bonding amide groups (**Ru-dpa**) increased the magnitude of ΔG°_{GS} (−0.41 and −0.44 eV) by 37−47% for bromide and chloride, respectively. Finally, the combination of alcohol and amide groups (**Ru-deaOH**) provided a 50% increase in ΔG°_{GS} (−0.45 eV) with both halides as compared to the **Ru-deeb** case.

Some apparent outliers are observed in this analysis, but these exceptions can be explained through consideration of the steric bulk or additional functional groups surrounding the amides. For example, **Ru-daeaOH** contains a terminal alcohol group but has a smaller K_{eq} value (3.5×10^6 M^{-1}) than **Ru-dpa** (2.8×10^7 M^{-1}), which has no terminal alcohol. The alcohol group of **Ru-daeaOH** was not resolved by ^{1}H NMR, which precluded the observation of interactions between the alcohol and the halide. However, halide interactions with the 3,3′ C−H and N−H bonds are significantly less than those of the other complexes, suggesting on average an increased distance between these groups and the halide. This is consistent with the amine group in the daeaOH ligand destabilizing the associated halide, which in turn lowers the K_{eq}. The drastically different equilibrium constants of **Ru-dpa** (2.8×10^7 M^{-1}) and **Ru-da** (5.7×10^5 M^{-1}) are also surprising, as both complexes have the same hydrogen-bonding functional groups. In the ^{1}H NMR spectrum of **Ru-dpa**, the aliphatic propyl resonances shift downfield with increasing halide concentration, indicating that this group contributes to halide association. The alkyl chain likely enhances the interaction by better encompassing the halide and preventing its dissociation. This suggests that tuning the sterics of the receptor ligand is important for optimal supramolecular assembly.

To summarize, in these complexes, contributions from molecular charge, hydrogen-bonding functional groups, and steric bulk all affect ground-state halide assembly in CH_2Cl_2. The inherent 2+ charge of the ruthenium complexes contributes significantly to halide binding in this solvent, while the amide functional groups provide a binding site that further stabilizes the halide. Additional functional groups such as alcohols can influence the halide location within the supramolecular assembly and enhance stability yet again. Finally, the appropriate steric bulk is important for allowing halides to approach the receptor site and for preventing their dissociation after assembly.

EXCITED-STATE SUPRAMOLECULAR ASSEMBLY

In a prior report, we showed that halide photorelease can be achieved with ruthenium complexes that form a 1:1 ion pair with chloride.[17] This behavior was clearly observed after pulsed-laser excitation of an ion-paired complex $[Ru^{2+},Cl^-]^+$ that resulted in time-dependent shifts in the PL spectra, consistent with chloride photorelease and PL from the free ruthenium complex. In that report, the excited-state dipole orientation was paramount for controlling the excited-state assembly with halides. Excited-state localization on the receptor ligand led to halide photorelease, while excited-state localization away from that ligand led to enhanced halide binding. In this study, the excited-state dipole is oriented toward the ester- or amide-functionalized ligands, leading to halide photorelease for all complexes except **Ru-deeb**. The differences in the excited-state kinetic and thermodynamic parameters (Figure 6) between complexes are here related to the functional groups on the receptor ligand.

Photoexcitation greatly affects the excited-state supramolecular assembly of all complexes, leading to photoinduced release of halides from the amide-containing complexes and enhanced binding in **Ru-deeb**. For instance, the PL maxima of the complexes as monitored by steady-state PL spectroscopy shift significantly during the course of chloride and bromide titrations. For the amide complexes, the PL blue-shifts up to 810 cm^{-1} and is accompanied by a 2−3-fold increase in intensity. For **Ru-deeb**, supramolecular assembly results in a slight red shift and a concurrent decrease in the PL intensity. The opposing PL shifts to low (**Ru-deeb**) or high (amide complexes) energy are due to the excited-state dipole orientation relative to the location of the halide.[17]

It has been shown for this class of complexes that the MLCT excited state is localized on a single ligand, and that ligand is the one which is most easily reduced.[52] These complexes were designed such that, in the MLCT excited-state, an electron resides on the amide- or ester-functionalized ligand, and this was confirmed through electrochemical experiments that showed that the first reduction potential of the complexes most closely aligned with $[Ru(bpy\text{-}CONHEt)_3]^{2+/+}$ (−880 mV vs NHE)[53] or $[Ru(deeb)_3]^{2+/+}$ (−720 mV vs NHE)[54] and not $[Ru(dtb)_3]^{2+/+}$ (−1000 mV vs NHE).[55] In the amide complexes, where the excited-state dipole is oriented toward the ligand that binds the halide, the MLCT excited state is destabilized by Coulombic repulsion with the halide, which results in a higher-energy PL.

For **Ru-deeb**, the MLCT excited state is localized on the deeb ligand. However, chloride does not associate directly with this ligand, but is instead in close proximity to the Ru(II) center. Therefore, upon absorption of a photon, the excited-state dipole is not directed toward the halide. Photoexcitation, which formally generates a Ru(III) metal, thereby increases the Coulombic attraction to the halide. This stabilizes the excited state, as manifest in the lower-energy PL spectrum. Concurrent with this red shift is a decrease in the PL intensity, which is caused by an increase in the nonradiative rate constants (k_{nr}) as predicted through the energy gap law and which has been reported previously.[22,39]

DOI: 10.1021/acs.inorgchem.8b03383
Inorg. Chem. 2019, 58, 3316−3328

The halide-induced shifts in the steady-state PL were used to calculate the excited-state binding constants (K^*_{eq}) through Förster cycle analysis (Figure S25). The K^*_{eq} values for the amide complexes were found to be at least an order of magnitude less than the ground-state K_{eq} values, as was expected based on the excited-state dipole orientation. For **Ru-deeb**, supramolecular assembly is stronger in the excited state by a factor of 2.

To assess how the excited-state orientation affects the equilibrium constants for supramolecular assembly, the difference in free energy between the ground and excited-state ion pairs ($\Delta G^0_{GS} - \Delta G^0_{ES}$) was calculated (Table 2). A negative value provides an estimate of the destabilization in the excited state, while a positive value is indicative of enhanced binding. For all of the amide complexes, the free energy of supramolecular halide assembly decreases in the excited state by -80 ± 10 meV. This shows that, upon excitation, a halide associated with the amide ligands of **Ru-deaOH**, **Ru-dpa**, **Ru-daeaOH**, or **Ru-da** will be destabilized by 80 meV, behavior that is attributed mainly to the Coulombic repulsion of the halide with the excited state. The different functional groups on these ligands have no discernible impact on the repulsion that is felt by the halide. Because of the similarities of the complexes, the electron density in the thermally equilibrated MLCT excited state is likely distributed primarily on the coordinating nitrogen atoms, as has been suggested for ruthenium polypyridyl complexes.[56] Additionally, the distance between the ion-paired halide and these nitrogen atoms does not vary significantly from complex to complex. As the small structural differences between ligands do not affect these contributors to the excited-state repulsion, photoexcitation reduces the free energy of halide binding by approximately the same amount in each complex. Thus, the trend in ground-state equilibrium constants (**Ru-da** < **Ru-daeaOH** < **Ru-dpa** < **Ru-deaOH**) is retained in the excited state.

Although the difference between the ground- and excited-state equilibria is controlled primarily by the excited-state localization, the kinetics of photorelease are sensitive to individual functional group variations between the ligands. Examination of these rate constants is beneficial to understand the observed photorelease. The rate constants for halide association, k^*_{12}, are all within error the same, and on the order of 1×10^{11} M^{-1} s^{-1}. This value is in agreement with the calculated diffusion limit as described in eq S1 (Appendix, Supporting Information).[57] This suggests that the association of the ruthenium complex and the halide in the excited state is diffusion-limited. Therefore, the K^*_{eq} values are determined by the rate constant for photorelease, k^*_{21}, for each complex. These rate constants correspond to halide dissociation from the ligand on the nanosecond to microsecond time scale. As halide release is a unimolecular reaction, the dissociation could proceed on the time scale of molecular vibrations (ps), but as the rate is much slower, a barrier for halide photorelease is inferred. This barrier likely involves solvent reorganization to solvate the ruthenium complex and the halide, but this contribution is expected to be approximately the same for all complexes. The energy required to break the hydrogen-bonding interactions between the receptor ligand and the halide is also expected to contribute to this barrier. In this series, k^*_{21} was found to increase in the order of **Ru-deaOH** < **Ru-dpa** < **Ru-daeaOH** < **Ru-da**. This implies that **Ru-deaOH** has the largest barrier for halide photorelease, while **Ru-da** has the lowest barrier. Unsurprisingly, the trend for increasing k^*_{21} is the opposite of that observed for the ground-state equilibrium constants. This reinforces the result that hydrogen-bonding functional groups significantly stabilize halide assemblies, as these interactions provide a significant barrier to halide release in the excited state.

The excited-state kinetics and thermodynamics discussed above pose many challenges that hinder anion photorelease in polar solvents such as CH_3CN or water. For example, supramolecular assembly is known to be inversely proportional to the dielectric of the solvent.[58] In fact, previous work on **Ru-deaOH** determined that K_{eq} with chloride in CH_3CN is 8.5×10^5 M^{-1},[15] as compared to the K_{eq} of 3.6×10^7 M^{-1} reported here in CH_2Cl_2. To even facilitate supramolecular assembly through hydrogen-bonding interactions in polar solvents, it would be necessary to design a complex with many strong hydrogen-bond donors that outcompete the solvent's ability to stabilize halide. However, the presence of these groups inevitably increases the barrier for halide photorelease. This approach would also adversely affect the halide dissociation rate constants (k_{21}). As the energy barrier for the halide release would necessarily be large, k_{21} would be slow, and so long-lived excited states would be needed to ensure that the halide would be released before relaxation to the ground state.

To address these challenges, it is helpful to look to the alkali and alkaline earth metal cation binding literature, where several strategies have been employed to photoinitiate metal release in polar solvents like water and CH_3CN. Many of the techniques offer varying degrees of reversibility. For instance, photoreactivity[59−62] (irreversible) or photoisomerization[63,64] (partially reversible) of cation receptors leads to large increases in cation concentrations in polar solvents and even under biological conditions. Completely reversible photorelease mechanisms, which are of particular interest to this work, have been achieved with rhenium bipyridine complexes bearing an azacrown-ether conjugated to the metal center.[65−69] In cation-binding studies in CH_3CN, pulsed-laser excitation of the assembly structures led to photorelease of the associated cations that was attributed to the conjugation of the azacrown nitrogen with the metal center. Upon MLCT (Re to bpy) excitation, this nitrogen contributed significant charge density to the metal center, weakening its interaction with the cation in the crown ether. In this case, photoexcitation not only provided an energy input to overcome the barrier for cation release but also directly reduced the barrier by weakening interactions that contributed to cation association. A similar strategy could be utilized to facilitate anion photorelease in polar solvents. If the specific functional groups that recognized anions also accepted significant charge density in the excited state, the intermolecular forces that contribute to anion assembly would inherently be weakened. This approach could lead to complexes that strongly bind halides in the ground state in polar solvents but which have a modest barrier to halide photorelease in the excited state.

CONCLUSIONS

A series of ruthenium polypyridyl complexes containing ester- or amide-functionalized bipyridine ligands formed strong assembly structures ($K_{eq} \geq 1 \times 10^5$ M^{-1}) with chloride and bromide in CH_2Cl_2. Amide and alcohol functional groups on the receptor ligand significantly enhanced the equilibrium constant, as compared to a complex (**Ru-deeb**) without these groups. This allowed K_{eq} to be tuned by over 2 orders of magnitude. Photoexcitation of the ion-paired complexes led to

DOI: 10.1021/acs.inorgchem.8b03383
Inorg. Chem. 2019, 58, 3316−3328

a modest enhancement in the equilibrium constant (K^*_{eq}) of **Ru-deeb**, while an order of magnitude decrease in K^*_{eq} was observed for the amide complexes. The decrease in K^*_{eq} resulted in the photorelease of associated halide ions. The excited-state rate constants for halide dissociation (k_{21}) were largest for the complexes with the fewest hydrogen-bond donors (**Ru-da**), while the presence of functional groups that stabilized halides contributed to an energy barrier that decreased the rate of photorelease. The results show that excited-state supramolecular assembly can be controlled through molecular design.

EXPERIMENTAL SECTION

Materials. Sulfuric acid (H_2SO_4, Fisher, 98%, certified ACS Plus), methanol (Fisher, certified ACS), chloroform (Fisher, certified ACS), ethanolamine (Sigma-Aldrich, ≥98%), acetone (Sigma-Aldrich, certified ACS), acetonitrile (CH_3CN, Burdick and Jackson, 99.98%), and dichloromethane (CH_2Cl_2, Burdick and Jackson, 99.98%) were used as received. Argon gas (Airgas, 99.998%) was passed through a Drierite drying tube before use. Ammonium hexafluorophosphate (NH_4PF_6, Sigma-Aldrich, ≥98%), tetrabutylammonium chloride (TBACl, Sigma-Aldrich, purum ≥97%), tetrabutylammonium bromide (TBABr, Acros Organics, 99+%), tetrabutylammonium perchlorate ($TBAClO_4$, Sigma-Aldrich, for electrochemical analysis, ≥99%), and ruthenium trichloride hydrate (Oakwood Chemicals, 97%) were used as received. NMR solvents were purchased from Cambridge Isotope Laboratories, Inc. Ru(dtb)$_2$Cl$_2$·2H$_2$O,[70] 4,4′-dicarboxy-2,2′-bipyridine,[71] 4,4′-dimethylester-2,2′-bipyridine,[15] 4,4′-diethylester-2,2′-bipyridine (deeb),[72] [Ru(dtb)$_2$(dea)](PF$_6$)$_2$, (**Ru-deaOH**),[15] and [Ru(dtb)$_2$(daea)](PF$_6$)$_2$ (**Ru-daeaOH**)[17] were synthesized according to previous procedures. All solutions were sparged with argon for at least 30 min before all titration and transient PL experiments.

Synthesis of Ligands. General method for synthesis of amide-functionalized ligands. To 4,4′-dimethylester- or 4,4′-diethylester-2,2′-bipyridine in methanol was added an excess of the appropriate amine. The mixture was refluxed for 4 h. When cooled, acetone was added to the mixture, and the solid was collected by vacuum filtration on a sintered glass frit. The precipitate was washed with excess acetone and dried under vacuum at 100 °C, yielding a white powder.

deaOH. Refluxing 4,4′-diethylester-2,2′-bipyridine (2.0 g, 6.7 mmol) and ethanolamine (10 mL, 166 mmol) in methanol (40 mL) yielded 1.7 g (77%) of deaOH. ^{1}H NMR (d_6-DMSO, 500 MHz): 8.91 (2H, t), 8.85 (2H, d), 8.78 (2H, s), 7.85 (2H, dd), 4.83 (2H, t), 3.55 (4H, m), 3.38 (4H, m).

dpaOH. Refluxing 4,4′-dimethylester-2,2′-bipyridine (1.0 g, 3.7 mmol) and 3-amino-1-propanol (5 mL, 83 mmol) in methanol (20 mL) yielded 1.1 g (92%) of dpaOH. ^{1}H NMR (d_6-DMSO, 600 MHz): 8.95 (2H, t), 8.87 (2H, d), 8.78 (2H, s), 7.85 (2H, dd), 4.52 (2H, t), 3.48 (4H, m), 3.36 (4H, m), 1.71 (4H, p). ^{13}C NMR (d_6-DMSO, 150 MHz): 164.57, 155.52, 150.07, 143.03, 121.95, 118.22, 58.56, 36.81, 32.24.

dpa. Refluxing diethylester-2,2′-bipyridine (0.5 g, 1.6 mmol) and propylamine (3 mL) in methanol (10 mL) yielded 0.292 g (54%) of dpa. ^{1}H NMR (d_6-DMSO, 500 MHz): 8.96 (2H, t), 8.87 (2H, d), 8.79 (2H, s), 7.85 (2H, dd), 3.26 (4H, m), 1.57 (4H, m), 0.91 (6H, t). ^{13}C NMR (d_6-DMSO, 150 MHz): 164.53, 155.53, 150.07, 143.09, 121.97, 118.22, 41.18, 22.26, 11.53.

daeaOH. Refluxing dimethylester-2,2′-bipyridine (1.0 g, 3.7 mmol) and 2-[(2-aminoethyl)amino]ethanolamine (5 mL, 49 mmol) in methanol (20 mL) yielded 1.1 g (72%) of daeaOH. ^{1}H NMR (d_6-DMSO, 500 MHz): 8.93 (2H, t), 8.86 (2H, d), 8.79 (2H, d), 7.85 (2H, dd), 4.48 (2H, t), 3.44 (4H, q), 3.38 (4H, q), 2.72 (4H, t), 2.60 (4H, t).

Synthesis of da. 4,4′-Dicarboxy-2,2′-bipyridine (10g, 41.0 mmol) was refluxed under argon overnight in thionyl chloride (100 mL). The solvent was then removed from the mixture under reduced pressure, and the residue was dissolved in toluene. NH_3(g) was bubbled through the reaction mixture for 1 h, causing a precipitate to form. The precipitate was filtered and then washed with a minimum amount of DMSO and, finally, with excess acetone. The final product was obtained as a white powder (4.3 g, 42%). ^{1}H NMR (d_6-DMSO, 600 MHz): 8.86 (2H, dd), 8.80 (2H, dd), 8.42 (2H, s), 7.87 (2H, dd), 7.79 (2H, s). ^{13}C NMR (d_6-DMSO, 150 MHz): 166.30, 155.62, 150.04, 142.80, 122.00, 118.53.

Synthesis of deeb. 4,4′-Dicarboxy-2,2′-bipyridine (5g, 20.5 mmol) and H_2SO_4 (5 mL) were refluxed in ethanol (100 mL) for 5 d. The reaction mixture was added to $CHCl_3$ (200 mL), and H_2O (150 mL) was added. The aqueous layer was extracted with $CHCl_3$. The organic fraction was dried with $MgSO_4$, and the solvent was removed under vacuum, yielding 5.28 g (85%) of deeb. ^{1}H NMR ($CDCl_3$, 500 MHz): 8.93 (2H, s), 8.85 (2H, d), 7.90 (2H, dd), 4.45 (4H, q), 1.43 (6H, t).

Synthesis of Ruthenium Complexes. General method for synthesis of ruthenium complexes **Ru-deaOH**, **Ru-dpaOH**, **Ru-dpa**, **Ru-daeaOH**, and **Ru-deeb**. To a 10 mL glass microwave vial was added Ru(dtb)$_2$Cl$_2$·2H$_2$O, 1 equiv of the appropriate ligand, and ∼5 mL of EtOH or a 1:1 mixture of H$_2$O/EtOH. The mixture was heated under microwave radiation by an Anton Paar Monowave 300 at 150 °C for 10 min. The red solution was filtered, and the solvent was removed by rotary evaporation. The resulting solid was dissolved in minimal H_2O, and a few drops of saturated aqueous NH_4PF_6 were added, causing a precipitate to form. The solid was collected with vacuum filtration, washed with excess H_2O, and dried under vacuum at 100 °C overnight, yielding a red solid.

[Ru(dtb)$_2$(deaOH)](PF$_6$)$_2$, (Ru-deaOH). Ru(dtb)$_2$Cl$_2$ (75 mg, 0.096 mmol), deaOH (32 mg, 0.097 mmol) and ∼5 mL of H$_2$O/EtOH (1:1) were heated at 150 °C for 10 min under microwave irradiation, yielding 86 mg (71%) of **Ru-deaOH**. ^{1}H NMR (CD_2Cl_2, 400 MHz): 8.95 (2H, s), 8.27 (4H, d), 7.83 (2H, dd), 7.77 (2H, d), 7.60 (2H, t), 7.57 (4H, q), 7.45 (4H, td), 3.78 (4H, m), 3.58 (4H, m), 2.86 (2H, s), 1.42 (18H, s), 1.40 (18H, s).

[Ru(dtb)$_2$(dpaOH)](PF$_6$)$_2$, (Ru-dpaOH). Ru(dtb)$_2$Cl$_2$ (75 mg, 0.096 mmol), dpaOH (34 mg, 0.095 mmol), and ∼5 mL of H$_2$O/EtOH were heated at 150 °C for 10 min under microwave irradiation, yielding 110 mg (89%) of **Ru-dpaOH**. ^{1}H NMR (CD_2Cl_2, 400 MHz): 8.84 (2H, d), 8.27 (4H, dd), 7.81 (2H, dd), 7.77 (2H, d), 7.72 (2H, t), 7.57 (2H, d), 7.53 (2H, d), 7.46 (2H, dd), 7.43 (2H, dd), 3.70 (4H, t), 3.61 (4H, q), 1.82 (4H, p), 1.43 (18 H, s) 1.41 (18 H). High-resolution mass spectrometry (HRMS) electrospray ionization mass spectrometry (ESI-MS). Calcd for $C_{54}H_{70}F_{12}N_8O_4P_2Ru_1Na_1$ ([M + Na]$^+$): m/z 1309.37. Found: m/z 1309.37.

[Ru(dtb)$_2$(dpa)](PF$_6$)$_2$, (Ru-dpa). Ru(dtb)$_2$Cl$_2$ (75 mg, 0.096 mmol), dpa (31 mg, 0.095 mmol), and ∼5 mL of H$_2$O/EtOH were heated at 150 °C for 10 min under microwave irradiation, yielding 80 mg (66%) of **Ru-dpa**. ^{1}H NMR (CD_3CN, 500 MHz): 8.91 (2H, d), 8.48 (4H, dd), 7.84 (2H, d), 7.70 (2H, dd), 7.54 (4H, dd), 7.51 (2H, t), 7.42 (2H, dd), 7.35 (2H, dd), 3.37 (m, 4H), 1.63 (4H, h), 1.41 (18h, s), 1.39 (18h, s), 0.96 (6H, t). HRMS (ESI-MS). Calcd for $C_{54}H_{70}F_6N_8O_2P_1Ru_1$ ([M]$^{2+}$): m/z 482.24. Found: m/z 482.23.

[Ru(dtb)$_2$(daeaOH)](PF$_6$)$_2$, (Ru-daeaOH). Ru(dtb)$_2$Cl$_2$ (75 mg, 0.096 mmol), daeaOH (40 mg, 0.096 mmol), and ∼5 mL of H$_2$O/EtOH (1:1) were heated at 150 °C for 10 min under microwave irradiation, yielding 96 mg (74%) of **Ru-daeaOH**. ^{1}H NMR (CD_3CN, 500 MHz): 9.02 (s, 2H), 8.48 (dd, 4H), 7.84 (d, 2H), 7.73 (d, 2H), 7.55 (d, 4H), 7.42 (dd, 2H), 7.35 (dd, 2H), 3.56 (t, 4H), 3.51 (m, 4H), 2.85 (t, 4H), 2.73 (t, 4H), 1.41 (s, 18H), 1.39 (s, 18H).

[Ru(dtb)$_2$(deeb)](PF$_6$)$_2$, (Ru-deeb). Ru(dtb)$_2$Cl$_2$ (100 mg, 0.141 mmol), deeb (42 mg, 0.140 mmol), and ∼5 mL of EtOH were heated at 150 °C for 10 min under microwave irradiation, yielding 144 mg (83%) of **Ru-deeb**. ^{1}H NMR (CD_3CN, 500 MHz): 9.02 (2H, d), 8.48 (4H, dd), 7.90 (2H, d), 7.83 (2H, dd), 7.52 (4H, dd), 7.42 (2H, dd), 7.34 (2H, dd), 4.45 (4H, q), 1.41 (24 H, m), 1.39 (18H, s). HRMS (ESI-MS). Calcd for $C_{52}H_{64}N_6O_4Ru_1$ ([M]2+): m/z 469.2. Found: m/z 469.2.

[Ru(dtb)$_2$(da)](PF$_6$)$_2$, (Ru-da). [Ru(dtb)$_2$Cl$_2$] (500 mg, 0.071 mmol) and da (188 mg, 0.078 mmol) were dissolved in 12 mL of a 1:1 H$_2$O/EtOH mixture and refluxed overnight under argon. After reaction, the mixture was brought to room temperature and

DOI: 10.1021/acs.inorgchem.8b03383
Inorg. Chem. 2019, 58, 3316−3328

evaporated to dryness under vacuum. The residue was dissolved in 5 mL of water, and upon addition of a saturated aqueous NH_4PF_6 solution, a precipitate formed. The precipitate was collected by filtration and purified by column chromatography on alumina using CH_3CN/H_2O mixture, yielding 341 mg (41%) of **Ru-da**. ^{1}H NMR (CD_2Cl_2, 500 MHz): 8.87 (2H, s), 8.27 (4H, dd), 7.83 (2H, dd), 7.79 (2H, d), 7.57 (2H, d), 7.54 (2H, d), 7.46 (2H, dd), 7.44 (2H, dd), 7.07 (2H, s), 6.02 (2H), 1.43 (18H, s), 1.41 (18H, s). HRMS (ESI-MS). Calcd for $C_{48}H_{58}F_{12}N_8O_2P_2Ru_1Na_1$ ($[M + Na]^+$): m/z 1193.29. Found: m/z 1193.29.

Nuclear Magnetic Resonance. Characteristic NMR spectra were obtained at room temperature on a Bruker Avance III 400, 500, or 600 MHz spectrometer. Solvent residual peaks were used as internal standards for ^{1}H (δ = 7.26 ppm for $CDCl_3$, 2.50 ppm for DMSO, 5.32 for CD_2Cl_2, 1.94 for CD_3CN) and ^{13}C (δ = 77.16 ppm for $CDCl_3$, 39.52 ppm for DMSO) chemical shift referencing. NMR spectra were processed using MNOVA.

Mass Spectrometry. Samples were analyzed with a hybrid LTQ FT (ICR 7T) (ThermoFisher) mass spectrometer. Samples were introduced via a micro-electrospray source at a flow rate of 3 μL/min. Xcalibur (ThermoFisher) was used to analyze the data. Each mass spectrum was averaged over 200 time domains. Electrospray source conditions were set as spray voltage 4.7 kV, sheath gas (nitrogen) 3 arb, auxiliary gas (nitrogen) 0 arb, sweep gas (nitrogen) 0 arb, capillary temperature 275 °C, capillary voltage 35 V, and tube lens voltage 110 V. The mass range was set to 150−2000 m/z. All measurements were recorded at a resolution setting of 100 000. Solutions were analyzed at 0.1 mg/mL or less based on responsiveness to the ESI mechanism. Low-resolution mass spectrometry (linear ion trap) provided independent verification of molecular weight distributions.

UV−Vis Absorption. UV−Vis absorption spectra were recorded on a Varian Cary 60 UV−vis spectrophotometer with a resolution of 1 nm.

Steady-State PL. Steady-state PL spectra were recorded on a Horiba Fluorolog 3 fluorimeter and corrected by calibration with a standard tungsten-halogen lamp. Samples were excited at 450 nm. The intensity was integrated for 0.1 s at 1 nm resolution and averaged over three scans. The PL quantum yields were measured by the optically dilute method using $[Ru(bpy)_3]Cl_2$ in acetonitrile (Φ = 0.062) as a quantum yield standard.[73]

Time-Resolved Photoluminescence. Time-resolved PL data were acquired on a nitrogen dye laser with excitation centered at 445 nm. Pulsed light excitation was achieved with a Photon Technology International (PTI) GL-301 dye laser that was pumped by a PTI GL-3300 nitrogen laser. The PL was detected by a Hamamatsu R928 PMT optically coupled to a ScienceTech Model 9010 monochromator terminated into a LeCroy Waverunner LT322 oscilloscope. Decays were monitored at the PL maximum and averaged over 180 scans. Nonradiative and radiative rate constants were calculated from the quantum yields ($\Phi = k_r/(k_r + k_{nr})$) and lifetimes ($\tau = 1/(k_r + k_{nr})$).

Transient Photoluminescence. Transient photoluminescence data were obtained on the nitrogen dye laser described above. Excited-state decay traces were obtained every 10 nm from 560 to 770 nm and averaged over 60 scans. The amplitude of each PL decay after a specific time delay from the laser pulse (45 ns to 3 μs at given intervals) was plotted versus the wavelength, and the data were normalized to give the transient PL spectra shown in Figure 5.

Excited-State Equilibrium. The square scheme analysis used to resolve the excited-state kinetics are described elsewhere.[31−33]

Electrochemistry. Square-wave voltammetry was performed with a BASi Epsilon potentiostat in a standard three-cell in CH_2Cl_2 electrolytes. The cells consisted of a platinum working electrode and a platinum mesh as an auxiliary electrode. A nonaqueous silver/silver chloride electrode (Pine) was used as a reference electrode that was referenced to an internal ferrocene (724 mV vs NHE)[74] or decamethylferrocene[75] ($Me_{10}Fc$) standard (250 mV vs NHE).

Halide Titrations. UV−Vis, PL, and time-resolved measurements were performed in CH_2Cl_2 or CH_3CN using ∼10 μM solutions of the ruthenium complexes. Titration measurements were performed for each of the spectroscopies with TBACl or TBABr through additions of 0.25 equiv. Throughout all titrations, the concentration of complexes remained unchanged. To do so, a stock solution of each complex with an absorbance of ∼0.1 at 450 nm (∼6−10 μM) in the desired solvent was prepared. The stock solution was transferred into a spectro-photometric quartz cuvette (5 mL). A titration solution was then prepared with 25 mL of the complex's stock solution. TBACl or TBABr were added to the stock solution to obtain the desired concentration of halide. These solutions were then titrated to the quartz cuvette.

To perform the competitive binding experiments with **Ru-deaOH** and **Ru-dpa**, ruthenium solutions with an absorbance of ∼0.1 at 450 nm were prepared as described above. The desired amount of competitor (TBA triflate for **Ru-deaOH**, TBA tetrafluoroborate for **Ru-dpa**) was then added to the ruthenium solution to give a stock solution that contained excess (0.280−1.19 mM) competitor concentration. Three stock solutions were prepared with a 50, 100, and 200:1 ratio of competitor to ruthenium. Then, 5 mL of the stock solution was transferred to a quartz cuvette. A titrating solution was also prepared by dissolving the desired amount of TBACl or TBABr in 10 mL of the stock solution. The observed equilibrium constant (K_{obs}) at each competitor concentration was used to determine the halide equilibrium constant (K_{eq}) with eq 1, and the three trials were averaged to give the reported values.

The ^{1}H NMR titrations were performed using a Bruker Avance III 500 MHz spectrometer equipped with a broadband inverse (BBI) probe using 1 mM ruthenium complex in 600 μL of deuterated solvent, and 0.25 equiv additions of TBACl or TBAI were added in 10 μL additions. The ruthenium concentration was kept unchanged through preparation of a titration solution that contained both the ruthenium complex and the desired halide. Each spectrum was averaged over 16 scans.

Data analysis for all experiments was performed using Origin 2017. Data fitting was preformed using a Levenberg−Marquardt iteration method. Benesi−Hildebrand type of analysis was performed in Mathematica, version 11.

■ ASSOCIATED CONTENT

Supporting Information

The Supporting Information is available free of charge on the ACS Publications website at DOI: 10.1021/acs.inorgchem.8b03383.

^{1}H and ^{13}C NMR and high-resolution mass spectra of the newly synthesized compounds. UV−Vis, PL, and ^{1}H NMR titrations in $C(H_3/D_3)CN$ and $C(H_2/D_2)Cl_2$ (PDF)

■ AUTHOR INFORMATION

Corresponding Author

*E-mail: gjmeyer@email.unc.edu.

ORCID

Ludovic Troian-Gautier: 0000-0002-7690-1361

Renato N. Sampaio: 0000-0002-7158-6470

Gerald J. Meyer: 0000-0002-4227-6393

Notes

The authors declare no competing financial interest.

■ ACKNOWLEDGMENTS

We acknowledge support from the National Science Foundation, Award No. CHE-1213357. M.D.T. acknowledges support from the National Science Foundation Graduate Research Fellowship Program under Grant No. DGE-1650116. L.T.-G. acknowledges the Belgian American Educational

DOI: 10.1021/acs.inorgchem.8b03383
Inorg. Chem. 2019, 58, 3316−3328

Foundation as well as the Bourse d'Excellence Wallonie-Bruxelles for generous support.

REFERENCES

(1) Beer, P. D.; Gale, P. A. Anion Recognition and Sensing: The State of the Art and Future Perspectives. *Angew. Chem., Int. Ed.* **2001**, *40*, 486−516.

(2) Barendt, T. A.; Ferreira, L.; Marques, I.; Félix, V.; Beer, P. D. Anion- and Sovent-Induced Rotary Dynamics and Sensing in a Perylene Diimide [3]Catenane. *J. Am. Chem. Soc.* **2017**, *139*, 9026−9037.

(3) Lim, J. Y. C.; Marques, I.; Félix, V.; Beer, P. D. A Chiral Halogen-Bonding [3]Rotaxane for the Recognition and Sensing of Biologically Relevant Dicarboxylate Anions. *Angew. Chem., Int. Ed.* **2018**, *57*, 584−588.

(4) Ramos, S.; Alcalde, E.; Doddi, G.; Mencarelli, P.; Pérez-García, L. Quantitative Evaluation of the Chloride Template Effect in the Formation of Dicationic [1_4]Imidazoliophanes. *J. Org. Chem.* **2002**, *67*, 8463−8468.

(5) Raheem, I. T.; Thiara, P. S.; Peterson, E. A.; Jacobsen, E. N. Enantioselective Pictet-Spengler-Type Cyclizations of Hydroxylactams: H-Bond Donor Caalysis by Anion Binding. *J. Am. Chem. Soc.* **2007**, *129*, 13404−13405.

(6) Reisman, S. E.; Doyle, A. G.; Jacobsen, E. N. Enantioselective Thiourea-Catalyzed Additions to Oxocarbenium Ions. *J. Am. Chem. Soc.* **2008**, *130*, 7198−7199.

(7) Brown, A. R.; Kuo, W. H.; Jacobsen, E. N. Enantioselective Catalytic α-Alkylation of Aldehydes via an S_N1 Pathway. *J. Am. Chem. Soc.* **2010**, *132*, 9286−9288.

(8) Birrell, J. A.; Desrosiers, J. N.; Jacobsen, E. N. Enantioselective Acylation of Silyl Ketene Acetals through Fluoride Anion-Binding Catalysis. *J. Am. Chem. Soc.* **2011**, *133*, 13872−13875.

(9) Koulov, A. V.; Lambert, T. N.; Shukla, R.; Jain, M.; Boon, J. M.; Smith, B. D.; Li, H.; Sheppard, D. N.; Joos, J. B.; Clare, J. P.; Davis, A. P. Chloride Transport Across Vesicle and Cell Membranes by Steroid-Based Receptors. *Angew. Chem., Int. Ed.* **2003**, *42*, 4931−4933.

(10) McNally, B. A.; Koulov, A. V.; Lambert, T. N.; Smith, B. D.; Joos, J. B.; Sisson, A. L.; Clare, J. P.; Sgarlata, V.; Judd, L. W.; Magro, G.; Davis, A. P. Structure-Activity Relationships in Cholapod Anion Carriers: Enhanced Transmembrane Chloride Transport through Substituent Tuning. *Chem. - Eur. J.* **2008**, *14*, 9599−9606.

(11) Hussain, S.; Brotherhood, P. R.; Judd, L. W.; Davis, A. P. Diaxial Diureido Decalins as Compact, Efficient, and Tunable Anion Transporters. *J. Am. Chem. Soc.* **2011**, *133*, 1614−1617.

(12) Berezin, S. K.; Davis, J. T. Catechols as Membrane Anion Transporters. *J. Am. Chem. Soc.* **2009**, *131*, 2458−2459.

(13) Sessler, J. L.; Eller, L. R.; Cho, W. S.; Nicolaou, S.; Aguilar, A.; Lee, J. T.; Lynch, V. M.; Magda, D. J. Synthesis, Anion-Binding Properties, and In Vitro Anticancer Activity of Prodigiosin Analogues. *Angew. Chem., Int. Ed.* **2005**, *44*, 5989−5992.

(14) Winstanley, K. J.; Allen, S. J.; Smith, D. K. Encapsulated Binding Sites-Synthetically Simple Receptors for the Binding and Transport of HCl. *Chem. Commun.* **2009**, 4299−4301.

(15) Troian-Gautier, L.; Beauvilliers, E. E.; Swords, W. B.; Meyer, G. J. Redox Active Ion-Paired Excited States Undergo Dynamic Electron Transfer. *J. Am. Chem. Soc.* **2016**, *138*, 16815−16826.

(16) Wehlin, S. A. M.; Troian-Gautier, L.; Sampaio, R. N.; Marcélis, L.; Meyer, G. J. Ter-Ionic Complex that Forms a Bond Upon Visible Light Absorption. *J. Am. Chem. Soc.* **2018**, *140*, 7799−7802.

(17) Turlington, M. D.; Troian-Gautier, L.; Sampaio, R. N.; Beauvilliers, E. E.; Meyer, G. J. Ligand Control of Supramolecular Chloride Photorelease. *Inorg. Chem.* **2018**, *57*, 5624−5631.

(18) Werber, J. R.; Osuji, C. O.; Elimelech, M. Materials for Next-Generation Desalination and Water Purification Membranes. *Nat. Rev. Mater.* **2016**, *1*, 1−15.

(19) White, W.; Sanborn, C. D.; Reiter, R. S.; Fabian, D. M.; Ardo, S. Observation of Photovoltaic Action from Photoacid-Modified Nafion Due to Light-Driven Ion Transport. *J. Am. Chem. Soc.* **2017**, *139*, 11726−11733.

(20) Cutting, G. R. Cystic Fibrosis Genetics: From Molecular Understanding to Clinical Application. *Nat. Rev. Genet.* **2015**, *16*, 45−56.

(21) Benesi, H. A.; Hildebrand, J. H. A Spectrophotometric Investigation of the Interaction of Iodine with Aromatic Hydrocarbons. *J. Am. Chem. Soc.* **1949**, *71*, 2703−2707.

(22) Ward, W. M.; Farnum, B. H.; Siegler, M.; Meyer, G. J. Chloride Ion-Pairing with Ru(II) Polypyridyl Compounds in Dichloromethane. *J. Phys. Chem. A* **2013**, *117*, 8883−8894.

(23) Tse, J. K. Y.; Giannetti, A. M.; Bradshaw, J. M. Thermodynamics of Calmodulin Trapping by Ca^{2+}/Calmodulin-Dependent Protein Kinase II: Subpicomolar K_d Determined Using Competition Titration Calorimetry. *Biochemistry* **2007**, *46*, 4017−4027.

(24) Bellelli, A.; Carey, J. *Reversible Ligand Binding: Theory and Experiment;* John Wiley and Sons, Inc.: Hoboken, NJ, 2018; p 1−30.

(25) Le, V. H.; Yanney, M.; McGuire, M.; Sygula, A.; Lewis, E. A. Thermodynamics of Host-Guest Interactions between Fullerenes and a Buckycatcher. *J. Phys. Chem. B* **2014**, *118*, 11956−11964.

(26) Marton, A.; Clark, C. C.; Srinivasan, R.; Freundlich, R. E.; Narducci Sarjeant, A. A.; Meyer, G. J. Static and Dynamic Quenching of Ru(II) Polypyridyl Excited States by Iodide. *Inorg. Chem.* **2006**, *45*, 362−369.

(27) Wehlin, S. A. M.; Troian-Gautier, L.; Li, G.; Meyer, G. J. Chloride Oxidation by Ruthenium Excited-States in Solution. *J. Am. Chem. Soc.* **2017**, *139*, 12903−12906.

(28) Li, G.; Ward, W. M.; Meyer, G. J. Visible Light Driven Nanosecond Bromide Oxidation by a Ru Complex with Subsequent Br-Br Bond Formation. *J. Am. Chem. Soc.* **2015**, *137*, 8321−8323.

(29) Li, G.; Brady, M. D.; Meyer, G. J. Visible Light Driven Bromide Oxidation and Ligand Substitution Photochemistry of a Ru Diimine Complex. *J. Am. Chem. Soc.* **2018**, *140*, 5447−5456.

(30) O'Donnell, R. M.; Sampaio, R. N.; Li, G.; Johansson, P. G.; Ward, C. L.; Meyer, G. J. Photoacidic and Photobasic Behavior of Transition Metal Compounds with Carboxylic Acid Group(s). *J. Am. Chem. Soc.* **2016**, *138*, 3891−3903.

(31) Loken, M. R.; Hayes, J. W.; Gohlke, J. R.; Brand, L. Excited-State Proton Transfer as a Biological Probe. Determination of Rate Constants by Means of Nanosecond Fluorometry. *Biochemistry* **1972**, *11*, 4779−4786.

(32) Demas, J. N. *Excited State Lifetime Measurements;* Demas, J. N., Ed.; Academic Press: New York, 1983; p 43.

(33) Laws, W. R.; Brand, L. Analysis of Two-State Excited-State Reactions. The Fluorescence Decay of 2-Naphthol. *J. Phys. Chem.* **1979**, *83*, 795−802.

(34) Ireland, J. F.; Wyatt, P. A. H. *Advances in Physical Organic Chemistry;* Gold, V., Ed.; Academic Press: New York, 1976; Vol. *12*, p 131.

(35) Lakowicz, J. R. *Principles of Fluorescence Spectroscopy,* 2nd ed.; Kluwer Academic/Plenum Publishers: New York, 1999.

(36) Arunan, E.; Desiraju, G. R.; Klein, R. A.; Sadlej, J.; Scheiner, S.; Alkorta, I.; Clary, D. C.; Crabtree, R. H.; Dannenberg, J. J.; Hobza, P.; Kjaergaard, H. G.; Legon, A. C.; Mennucci, B.; Nesbitt, D. J. Definition of the Hydrogen Bond (IUPAC Recommendations 2011). *Pure Appl. Chem.* **2011**, *83*, 1637−1641.

(37) Bondy, C. R.; Loeb, S. J. Amide Based Receptors for Anions. *Coord. Chem. Rev.* **2003**, *240*, 77−99.

(38) Swords, W. B.; Li, G.; Meyer, G. J. Iodide Ion Pairing with Highly Charged Ruthenium Polypyridyl Cations in CH_3CN. *Inorg. Chem.* **2015**, *54*, 4512−4519.

(39) Troian-Gautier, L.; Wehlin, S. A. M.; Meyer, G. J. Photophysical Properties of Tetracationic Ruthenium Complexes and their Ter-Ionic Assemblies with Chloride. *Inorg. Chem.* **2018**, *57*, 12232−12244.

(40) Ramalingam, V.; Domaradzki, M. E.; Jang, S.; Muthyala, R. S. Carbonyl Groups as Molecular Valves to Regulate Chloride Binding to Squaramides. *Org. Lett.* **2008**, *10*, 7946−7949.

DOI: 10.1021/acs.inorgchem.8b03383
Inorg. Chem. 2019, 58, 3316−3328

(41) Amendola, V.; Bergamaschi, G.; Boiocchi, M.; Fabbrizzi, L.; Milani, M. The Squaramide Versus Urea Contest for Anion Recognition. *Chem. - Eur. J.* **2010**, *16*, 4368−4380.
(42) Bondy, C. R.; Gale, P. A.; Loeb, S. J. Platinum(II) Nicotinamide Complexes as Receptors for Oxo-Anions. *Chem. Commun.* **2001**, 729−730.
(43) Beer, P. D.; Szemes, F.; Balzani, V.; Salà, C. M.; Drew, M. G. B.; Dent, S. W.; Maestri, M. Anion Selective Recognition and Sensing by Novel Macrocyclic Transition Metal Receptor Systems. ^{1}H NMR, Electrochemical, and Photophysical Investigations. *J. Am. Chem. Soc.* **1997**, *119*, 11864−11875.
(44) Szemes, F.; Hesek, D.; Chen, Z.; Dent, S. W.; Drew, M. G. B.; Goulden, A. J.; Graydon, A. R.; Grieve, A.; Mortimer, R. J.; Wear, T.; Weightman, J. S.; Beer, P. D. Synthesis and Characterization of Novel Acyclic, Macrocyclic, and Calix[4]arene Ruthenium(II) Bipyridyl Receptor Molecules that Recognize and Sense Anions. *Inorg. Chem.* **1996**, *35*, 5868−5879.
(45) Beer, P. D.; Dent, S. W.; Wear, T. J. Spectral and Electrochemical Recognition of Halide Anions by Acyclic Mononuclear Ruthenium(II) Bipyridyl Receptor Molecules. *J. Chem. Soc., Dalton Trans.* **1996**, 2341−2346.
(46) Smith, D. K. Rapid NMR Screening of Chloride Receptors: Uncovering Catechol as a Useful Anion Binding Motif. *Org. Biomol. Chem.* **2003**, *1*, 3874−3877.
(47) Winstanley, K. J.; Sayer, A. M.; Smith, D. K. Anion Binding by Catechols-an NMR, Optical and Electrochemical Study. *Org. Biomol. Chem.* **2006**, *4*, 1760−1767.
(48) Li, Y.; Flood, A. H. Pure C-H Hydrogen Bonding to Chloride Ions: A Preorganized and Rigid Macrocyclic Receptor. *Angew. Chem., Int. Ed.* **2008**, *47*, 2649−2652.
(49) Li, Y.; Flood, A. H. Strong, Size-Selective, and Electronically Tunable C-H●●●Halide Binding with Steric Control over Aggregation from Synthetically Modular, Shape-Persistent [3_4]-Triazolophanes. *J. Am. Chem. Soc.* **2008**, *130*, 12111−12122.
(50) Meudtner, R. M.; Hecht, S. Helicity Inversion in Responsive Foldamers Induced by Achiral Halide Ion Guests. *Angew. Chem., Int. Ed.* **2008**, *47*, 4926−4930.
(51) Juwarker, H.; Lenhardt, J. M.; Pham, D. M.; Craig, S. L. 1,2,3-Triazole CH●●●Cl^{-} Contacts Guide Anion Binding and Concomitant Folding in 1,4-Diaryl Triazole Oligomers. *Angew. Chem., Int. Ed.* **2008**, *47*, 3740−3743.
(52) Blakley, R. L.; Dearmond, M. K. Unique Spectroscopic Properties of Mixed-Ligand Complexes with 2,2'-Dipyridylamine: A Dual Luminescence from a Ruthenium(II) Complex. *J. Am. Chem. Soc.* **1987**, *109*, 4895−4901.
(53) Elliott, C. M.; Hershenhart, E. J. Electrochemical and Spectral Investigations of Ring-Substituted Bipyridine Complexes of Ruthenium. *J. Am. Chem. Soc.* **1982**, *104*, 7519−7526.
(54) Farnum, B. H.; Gardner, J. M.; Marton, A.; Narducci-Sarjeant, A. A.; Meyer, G. J. Influence of Ion Pairing on the Oxidation of Iodide by MLCT Excited States. *Dalt. Trans.* **2011**, *40*, 3830−3838.
(55) Rota Martir, D.; Averardi, M.; Escudero, D.; Jacquemin, D.; Zysman-Colman, E. Photoinduced Electron Transfer in Supramolecular Ruthenium-Porphyrin Assemblies. *Dalton Trans.* **2017**, *46*, 2255−2262.
(56) Oh, D. H.; Boxer, S. G. Stark Effect Spectra of Ru(diimine)$_3^{2+}$ Complexes. *J. Am. Chem. Soc.* **1989**, *111*, 1131−1133.
(57) Gardner, J. M.; Abrahamsson, M.; Farnum, B. H.; Meyer, G. J. Visible Light Generation of Iodine Atoms and I-I Bonds: Sensitized I^{-} Oxidation and I_3^{-} Photodissociation. *J. Am. Chem. Soc.* **2009**, *131*, 16206−16214.
(58) Liu, Y.; Sengupta, A.; Raghavachari, K.; Flood, A. H. Anion Binding in Solution: Beyond the Electrostatic Regime. *Chem.* **2017**, *3*, 411−427.
(59) Adams, S. R.; Kao, J. P. Y.; Grynkiewicz, G.; Minta, A.; Tsien, R. Y. Biologically Useful Chelators that Release Ca^{2+} upon Illumination. *J. Am. Chem. Soc.* **1988**, *110*, 3212−3220.
(60) Kimura, K.; Mizutani, R.; Yokoyama, M.; Arakawa, R.; Sakurai, Y. Metal-Ion Complexation and Photochromism of Triphenylmethane Dye Derivatives Incorporating Monoaza-15-crown Moieties. *J. Am. Chem. Soc.* **2000**, *122*, 5448−5454.
(61) Kaplan, J. H.; Ellis-Davies, G. C. R. Photolabile Chelators for the Rapid Photorelease of Divalent Cations. *Proc. Natl. Acad. Sci. U. S. A.* **1988**, *85*, 6571−6575.
(62) Cui, J.; Gropeanu, R. A.; Stevens, D. R.; Rettig, J.; Campo, A. New Photolabile BAPTA-Based Ca^{2+} Cages with Improved Photorelease. *J. Am. Chem. Soc.* **2012**, *134* (18), 7733−7740.
(63) Lednev, I. K.; Hester, R. E.; Moore, J. N. Direct Observation of Photocontrolled Ion Release: A Nanosecond Time-Resolved Spectroscopic Study of a Benzothiazolium Styryl Azacrown Ether Dye Complexed with Barium. *J. Phys. Chem. A* **1997**, *101*, 7371−7378.
(64) Malval, J. P.; Gosse, I.; Morand, J. P.; Lapouyade, R. Photoswitching of Cation Complexation with a Monoaza-crown Dithienylethene Photochrome. *J. Am. Chem. Soc.* **2002**, *124*, 904−905.
(65) MacQueen, D. B.; Schanze, K. S. Cation-Controlled Photophysics in a Re(I) Fluoroionophore. *J. Am. Chem. Soc.* **1991**, *113*, 6108−6110.
(66) Lewis, J. D.; Moore, J. N. Photoinduced Ba^{2+} Release and Thermal Rebinding by an Azacrown Ether Linked by an Alkynyl Pyridine to a (bpy)Re(CO)$_3$ Group. *Chem. Commun.* **2003**, 2858−2859.
(67) Lewis, J. D.; Perutz, R. N.; Moore, J. N. Light-Controlled Ion Swithcing: Direct Observation of the Complete Nanosecond Release and Microsecond Recapture Cycle of an Azacrown-Substituted [(bpy)Re(CO)$_3$L]$^{+}$ Complex. *J. Phys. Chem. A* **2004**, *108*, 9037−9047.
(68) Lewis, J. D.; Clark, I. P.; Moore, J. N. Ground and Excited State Resonance Raman Spectra of an Azacrown-Substituted [(bpy)Re(CO)$_3$L]$^{+}$ Complex: Characterization of Excited States, Determination of Sturcture and Bonding, and Observation of Metal Cation Release from the Azacrown. *J. Phys. Chem. A* **2007**, *111*, 50−58.
(69) Lewis, J. D.; Towrie, M.; Moore, J. N. Ground- and Excited-State Infrared Spectra of an Azacrown-Substituted [(bpy)Re(CO)$_3$L]$^{+}$ Complex: Sturcture and Bonding in Ground and Excited States and Effects of Ba^{2+} Binding. *J. Phys. Chem. A* **2008**, *112*, 3852−3864.
(70) Hadda, T. B.; Le Bozec, H. Preparation and Characterization of Ruthenium Complexes with the New 4,4',4''-tri-*tert*-butyl-terpyridine Ligand and with 4,4'-di-*tert*-butyl-bipyridine. *Polyhedron* **1988**, *7*, 575−577.
(71) Hoertz, P. G.; Staniszewski, A.; Marton, A.; Higgins, G. T.; Incarvito, C. D.; Rheingold, A. L.; Meyer, G. J. Toward Exceeding the Shockley-Queisser Limit: Photoinduced Interfacial Charge Transfer Processes that Store Energy in Excess of the Equilibrated Excited State. *J. Am. Chem. Soc.* **2006**, *128*, 8234−8245.
(72) Gillaizeau-Gauthier, I.; Odobel, F.; Alebbi, M.; Argazzi, R.; Costa, E.; Bignozzi, C. A.; Qu, P.; Meyer, G. J. Phosphonate-Based Bipyridine Dyes for Stable Photovoltaic Devices. *Inorg. Chem.* **2001**, *40*, 6073−6079.
(73) Crosby, G. A.; Demas, J. N. The Measurement of Photoluminescence Quantum Yields. A Review. *J. Phys. Chem.* **1971**, *75*, 991−1024.
(74) Connelly, N. G.; Geiger, W. E. Chemical Redox Agents for Organometallic Chemistry. *Chem. Rev.* **1996**, *96*, 877−910.
(75) Noviandri, I.; Brown, K. N.; Fleming, D. S.; Gulyas, P. T.; Lay, P. A.; Masters, A. F.; Phillips, L. The Decamethylferrocenium/Decamethylferrocene Redox Couple: A Superior Redox Standard to the Ferrocenium/Ferrocene Redox Couple for Studying Solvent Effects on the Thermodynamics of Electron Transfer. *J. Phys. Chem. B* **1999**, *103*, 6713−6722.

DOI: 10.1021/acs.inorgchem.8b03383
Inorg. Chem. 2019, 58, 3316−3328